GEOPHYSICS, VOL. 76, NO. 4 (JULY-AUGUST 2011); P. SA63–SA76, 16 FIGS., 1 TABLE.
10.1190/1.3580633

Controlled-source interferometric redatuming by crosscorrelation and multidimensional deconvolution in elastic media

Joost van der Neut[1], Jan Thorbecke[1], Kurang Mehta[2], Evert Slob[1], and Kees Wapenaar[1]

ABSTRACT

Various researchers have shown that accurate redatuming of controlled seismic sources to downhole receiver locations can be achieved without requiring a velocity model. By placing receivers in a horizontal or deviated well and turning them into virtual sources, accurate images can be obtained even below a complex near-subsurface. Examples include controlled-source interferometry and the virtual-source method, both based on crosscorrelated signals at two downhole receiver locations, stacked over source locations at the surface. Because the required redatuming operators are taken directly from the data, even multiple scattered waveforms can be focused at the virtual-source location, and accurate redatuming can be achieved. To reach such precision in a solid earth, representations for elastic wave propagation that require multicomponent sources and receivers must be implemented. Wavefield decomposition prior to crosscorrelation allows us to enforce virtual sources to radiate only downward or only upward. Virtual-source focusing and undesired multiples from the overburden can be diagnosed with the interferometric point-spread function (PSF), which can be obtained directly from the data if an array of subsurface receivers is deployed. The quality of retrieved responses can be improved by filtering with the inverse of the PSF, a methodology referred to as multidimensional deconvolution.

INTRODUCTION

Researchers have shown how seismic data can be redatumed from the acquisition level to an arbitrary level in the subsurface by crosscorrelating the data with redatuming operators (Berryhill, 1979; Tegtmeier et al., 2004) or through a more rigorous matrix inversion (Mulder, 2005). These methods generally require a velocity model to compute the redatuming operators. Alternatively, the operators can be estimated iteratively from surface seismic data, as done in common-focus-point (CFP) technology (Berkhout, 1997; Thorbecke, 1997; Kelamis et al., 2002). When seismic receivers are placed in boreholes in the subsurface, the required operators can be measured directly. This is the key idea behind controlled-source seismic interferometry (Schuster and Zhou, 2006; Schuster, 2009) and the virtual-source method (Bakulin and Calvert, 2006; Korneev and Bakulin, 2006).

The use of actual subsurface receivers allows us to obtain the redatuming operators much more accurately than in any model-driven approach without having to rely on a velocity model. Therefore, data-driven redatuming is especially interesting below complex structures in the near-subsurface, where accurate velocity models are hard to obtain and transmitted wavefields tend to be strongly distorted (Bakulin et al., 2007b). Because all waveforms are actually measured, even multiple scattered wavefields can be focused (Vasconcelos et al., 2008).

Various interferometry representations have been derived from acoustic-wave theory. A few researchers have applied the concept for shear waves. Bakulin et al. (2007a) and Poletto et al. (2008) generate virtual shear-wave sources from walkaway vertical seismic profiling (VSP) data. Xiao et al. (2006) delineate salt flanks by crosscorrelating P- and S-wave arrivals in VSP data. Wapenaar (2004) and van Manen et al. (2006) derive interferometric representations to retrieve an exact Green's function in elastic media. Similar relations are applied to ocean-bottom cable (OBC) data by Gaiser and Vasconcelos (2010) and to VSP data by Gaiser et al. (2009).

Decomposing up- and downgoing wavefields prior to crosscorrelation can significantly improve interferometric redatuming, as shown by Mehta et al. (2007). In this paper, we generalize this concept for elastic media, where acoustic decomposition is replaced by elastic decomposition, separating the recordings into

Manuscript received by the Editor 12 August 2010; revised manuscript received 17 December 2010; published online 3 June 2011.
[1]Delft University of Technology, Department of Geotechnology, Delft, The Netherlands. E-mail: j.r.vanderneut@tudelft.nl; j.w.thorbecke@tudelft.nl; e.c.slob@tudelft.nl; c.p.a.wapenaar@tudelft.nl.
[2]Shell International Exploration & Production Inc., Houston, Texas, U.S.A. E-mail: kurang.mehta@shell.com.

up- and downgoing P- and S-wave constituents. We show how virtual sources can be generated that emit only one particular wave mode, either downward or upward.

From a theoretical view, redatuming by crosscorrelation has its limitations. First, free-surface interactions are assumed to have been eliminated. This condition can be relaxed when volume-force sources and deformation-rate sources are deployed (Wapenaar, 2004). Second, the concept generally is applied with one-sided illumination, meaning that sources are located at the earth's surface only instead of, as theory prescribes, on a closed integral surrounding the downhole receivers (Wapenaar, 2006). Third, the theory assumes lossless media (Snieder, 2007).

For these reasons, alternative redatuming schemes have been proposed, based on wavefield deconvolution (Bakulin and Calvert, 2006; Snieder et al., 2006; Vasconcelos and Snieder, 2008; Poletto et al., 2010). Schuster and Zhou (2006) and Wapenaar et al. (2008a) show that to obtain an exact Green's function obeying 3D wave propagation, multidimensional deconvoluion (MDD) should be implemented instead of trace-to-trace deconvolution. Applying MDD changes the boundary conditions, such that a reflection response is retrieved as if the medium above the receivers were homogeneous. In this way, all interaction effects with the medium above the receivers, including multiples, can be eliminated. The concept is similar to Betti deconvolution as applied by Amundsen et al. (2001) and Holvik and Amundsen (2005) to remove multiple reflections from OBC data. Here, we demonstrate that interferometric redatuming of controlled sources to downhole receivers can benefit significantly from such an approach.

We briefly review interferometric representations by crosscorrelation of two-way wavefields in elastic media. Then we derive alternative solutions for one-way wavefields, allowing us to steer virtual sources in the direction of our interest. We show how multidimensional deconvolution can further improve the redatumed responses, and we discuss the interferometric point-spread function (PSF) that can be used to diagnose the quality of virtual-source focusing and predict undesired multiples that can populate retrieved gathers. Finally, we illustrate these theories with synthetic examples of a layered lossless medium, a layered dissipative medium, and a complex inhomogeneous medium.

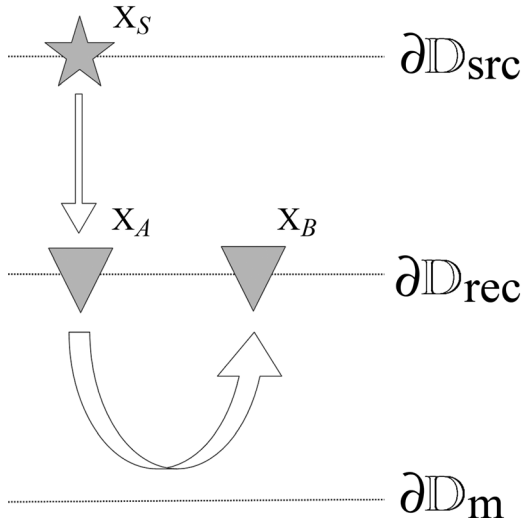

Figure 1. Configuration for interferometric redatuming. Sources are located at $\mathbf{x}_S$ at level $\partial\mathbb{D}_{\text{src}}$, and receivers are located at $\mathbf{x}_A$ and $\mathbf{x}_B$ at level $\partial\mathbb{D}_{\text{rec}}$, where receiver $\mathbf{x}_A$ is turned into a virtual source. Level $\partial\mathbb{D}_m$ is located below the deepest scatterer in the medium.

ELASTIC INTERFEROMETRY BY CROSSCORRELATION OF TWO-WAY WAVEFIELDS

In the following discussion, vectors are indicated in bold, where $\mathbf{x}=(x_1,x_1,x_3)^T$ denotes a location in a Cartesian coordinate system and superscript T is the transpose. The summation convention is applied to lowercase subscripts, meaning that repeated subscripts are implicitly summed over. A typical configuration for interferometric redatuming is shown in Figure 1. The aim is to redatum multicomponent sources from the earth's surface $\partial\mathbb{D}_{\text{src}}$ to receiver level $\partial\mathbb{D}_{\text{rec}}$. The main difference with common model-driven approaches is that in our case physical receivers are located at $\partial\mathbb{D}_{\text{rec}}$, allowing us to measure the redatuming operators between $\partial\mathbb{D}_{\text{src}}$ to $\partial\mathbb{D}_{\text{rec}}$ very accurately. Wapenaar (2004) shows that for redatuming in elastic media, it is desirable to decompose wavefields at the source side prior to crosscorrelation. This means that P- or S-wave sources should be generated from horizontal and vertical vibrator sources through a procedure outlined by Wapenaar et al. (1990).

Next, an approximation of the band-limited Green's function between receiver locations $\mathbf{x}_A$ and $\mathbf{x}_B$ and its acausal counterpart can be retrieved by evaluating

$$\hat{S}_0(\omega)[\hat{G}_{p,q}(\mathbf{x}_B,\mathbf{x}_A,\omega)+\{\hat{G}_{p,q}(\mathbf{x}_B,\mathbf{x}_A,\omega)\}^*] \approx \frac{2}{\rho c^k}\int_{\partial\mathbb{D}_{\text{src}}}\hat{F}^k(\mathbf{x}_S,\omega)\hat{v}_{p,k}(\mathbf{x}_B,\mathbf{x}_S,\omega)\{\hat{v}_{q,k}(\mathbf{x}_A,\mathbf{x}_S,\omega)\}^* d\mathbf{x}_S. \quad (1)$$

On the right side, we find $\hat{v}_{q,k}(\mathbf{x}_A,\mathbf{x}_S,\omega)$, denoting the observed q-component of the particle velocity at $\mathbf{x}_A$ from a decomposed k-component source at $\mathbf{x}_S$, where $k=1$ denotes a P-wave source and $k=2$ or $k=3$ denotes an S-wave source. The quantity $\hat{v}_{p,k}(\mathbf{x}_B,\mathbf{x}_S,\omega)$ is the observed p-component of the particle velocity at $\mathbf{x}_B$ resulting from the same source. The carets denote the frequency domain, asterisks denote complex conjugation, and ω is the angular frequency. The quantity $\hat{F}^k(\mathbf{x}_S,\omega)=\hat{S}_0(\omega)/(|\hat{S}^k(\mathbf{x}_S,\omega)|^2+\varepsilon^2)$ is a wavelet shaping filter, where $\hat{S}^k(\mathbf{x}_S,\omega)$ is the spectrum of an individual source, $\hat{S}_0(\omega)$ is the desired wavelet of the output data, and ε is a constant for deconvolution stability. The quantities ρ and c^k are the density and propagation velocity of the corresponding wave type: for P-wave sources, $c^k=c^{\text{P}}$ is the P-wave velocity; for S-wave sources, $c^k=c^S$ is the S-wave velocity. Superscript k takes the value of subscript k when the summation convention is applied. It is assumed that the medium properties are constant at the source array. The retrieved response $\hat{G}_{p,q}(\mathbf{x}_B,\mathbf{x}_A,\omega)+\{\hat{G}_{p,q}(\mathbf{x}_B,\mathbf{x}_A,\omega)\}^*$ represents a Green's function and its acausal counterpart as if there were a q-component virtual force source at $\mathbf{x}_A$ and the p-component of particle velocity registered at $\mathbf{x}_B$.

To retrieve an accurate response with equation 1, the medium should be homogeneous above the source array (Wapenaar,

2004). Because interactions with the free surface are not accounted for, these should be removed prior to crosscorrelation. Further, the medium should be lossless (Snieder, 2007), recording times should be sufficiently long to capture entire signals, and enough scattering must be assumed below the receivers to compensate for the one-sided illumination (Wapenaar, 2006).

ELASTIC INTERFEROMETRY BY CROSSCORRELATION OF ONE-WAY WAVEFIELDS

If multiple and/or multicomponent receivers are available in the borehole, wavefield decomposition can be applied to separate up- and downgoing P- and S-waves prior to crosscorrelation. It is important to note that we define our coordinate system with respect to the well trajectory.

The situation is shown in Figure 2, where the $\mathbf{i}_1$-direction is chosen parallel to the well. Curved well trajectories can be taken into account by choosing curvilinear coordinate systems (Frijlink and Wapenaar, 2010). The plane spanned by source and receivers is similar to the plane spanned by $\mathbf{i}_1$ and $\mathbf{i}_3$. Various researchers have shown how wavefields can be decomposed into P- and S-wave constituents propagating in positive and negative $\mathbf{i}_1$-directions (Leaney, 1990; Sun et al., 2009). For interferometric redatuming of controlled sources to receiver locations in horizontal or deviated wells, we generally aim to distinguish P- and S-waves propagating in the positive $\mathbf{i}_3$-direction, defined as downgoing, from those propagating in the negative $\mathbf{i}_3$-direction, defined as upgoing. In Appendix A, we show how such so-called one-way fields can be obtained.

In Appendix B, we derive a Green's function representation for seismic interferometry by crosscorrelation of one-way fields. We show that crosscorrelation of $\hat{P}^{+,+}_{n,k}(\mathbf{x}_A,\mathbf{x}_S,\omega)$ (being the n-component of the downgoing field at $\mathbf{x}_A$ coming from a source for downgoing k-mode waves at $\mathbf{x}_S$) and $\hat{P}^{-,+}_{m,k}(\mathbf{x}_B,\mathbf{x}_S,\omega)$ (being the m-component of the upgoing field at $\mathbf{x}_B$ coming from a source for downgoing k-mode waves at $\mathbf{x}_S$) yields

$$\hat{S}_0(\omega)\left[\hat{G}^{-,+}_{m,n}(\mathbf{x}_B,\mathbf{x}_A,\omega)-\{\hat{G}^{+,-}_{n,m}(\mathbf{x}_A,\mathbf{x}_B,\omega)\}^*\right]\approx\int_{\partial\mathbb{D}_{\mathrm{src}}}\hat{F}^k(\mathbf{x}_S,\omega)\hat{P}^{-,+}_{m,k}(\mathbf{x}_B,\mathbf{x}_S,\omega)\{\hat{P}^{+,+}_{n,k}(\mathbf{x}_A,\mathbf{x}_S,\omega)\}^*d\mathbf{x}_S. \tag{2}$$

Here, $\hat{F}^k(\mathbf{x}_S,\omega)$ is the same shaping filter as in equation 1. Note that the redatumed response is asymmetric. The quantity $\hat{G}^{-,+}_{m,n}(\mathbf{x}_B,\mathbf{x}_A,\omega)$ is the response as if there were a downgoing P-wave ($n=1$) or S-wave ($n=2$ or $n=3$) emitted at $\mathbf{x}_A$ and an upgoing P-wave ($m=1$) or S-wave ($m=2$ or $m=3$) received at $\mathbf{x}_B$. The quantity $\hat{G}^{+,-}_{n,m}(\mathbf{x}_A,\mathbf{x}_B,\omega)$ is the response as if there were an upgoing P- or S-wave emitted at $\mathbf{x}_B$ and a downgoing P- or S-wave received at $\mathbf{x}_A$. By taking the causal part of equation 2 in the time domain, we can retrieve the responses of downward-radiating virtual sources at $\mathbf{x}_A$.

Similarly, crosscorrelation of $\hat{P}^{-,+}_{n,k}(\mathbf{x}_A,\mathbf{x}_S,\omega)$ (being the n-component of the upgoing field at $\mathbf{x}_A$ coming from a source for downgoing k-mode waves at $\mathbf{x}_S$) and $\hat{P}^{+,+}_{m,k}(\mathbf{x}_B,\mathbf{x}_S,\omega)$ (being the m-component of the downgoing field at $\mathbf{x}_B$ coming from a source for downgoing k-mode waves at $\mathbf{x}_S$) yields

$$\hat{S}_0(\omega)\left[\hat{G}^{+,-}_{m,n}(\mathbf{x}_B,\mathbf{x}_A,\omega)-\{\hat{G}^{-,+}_{n,m}(\mathbf{x}_A,\mathbf{x}_B,\omega)\}^*\right]\approx-\int_{\partial\mathbb{D}_{\mathrm{src}}}\hat{F}^k(\mathbf{x}_S,\omega)\hat{P}^{+,+}_{m,k}(\mathbf{x}_B,\mathbf{x}_S,\omega)\{\hat{P}^{-,+}_{n,k}(\mathbf{x}_A,\mathbf{x}_S,\omega)\}^*d\mathbf{x}_S. \tag{3}$$

The quantity $\hat{G}^{+,-}_{m,n}(\mathbf{x}_B,\mathbf{x}_A,\omega)$ denotes the response as if there were an upgoing P- or S-wave emitted at $\mathbf{x}_A$ and a downgoing P- or S-wave received at $\mathbf{x}_B$. The quantity $\hat{G}^{-,+}_{n,m}(\mathbf{x}_A,\mathbf{x}_B,\omega)$ denotes the response as if there were a downgoing P- or S-wave emitted at $\mathbf{x}_B$ and an upgoing P- or S-wave registered at $\mathbf{x}_A$. By taking the causal part of equation 2, we can retrieve the responses of upward-radiating virtual sources at $\mathbf{x}_A$. Because of one-way reciprocity, the acausal part of equation 2 is equal to the complex conjugate of the causal part of equation 3, and vice versa.

ELASTIC INTERFEROMETRY BY MULTIDIMENSIONAL DECONVOLUTION

In the introduction, we mention several reasons why crosscorrelation does not always provide the most desirable reflection response. An alternative approach is taken by Wapenaar et al. (2008a) by interpreting interferometry as an inverse problem. Based on the decomposed wavefields discussed in Appendix A, a forward problem can be derived:

$$\hat{P}^{-,+}_{m,k}(\mathbf{x}_B,\mathbf{x}_S,\omega)=\int_{\mathbb{D}_{\mathrm{rec}}}\hat{\tilde{G}}^{-,+}_{m,n}(\mathbf{x}_B,\mathbf{x}_A,\omega)\hat{P}^{+,+}_{n,k}(\mathbf{x}_A,\mathbf{x}_S,\omega)d\mathbf{x}_A, \tag{4}$$

where the integration takes place over receiver coordinates $\mathbf{x}_A$ and where receiver component n is implicitly summed over by the summation convention. The quantity $\hat{\tilde{G}}^{-,+}_{m,n}(\mathbf{x}_B,\mathbf{x}_A,\omega)$ is the response that would be recorded if there were a downgoing n-component virtual source at $\mathbf{x}_A$ and an upgoing m-component field registered at $\mathbf{x}_B$, where n and m stand for P- or S-waves, as

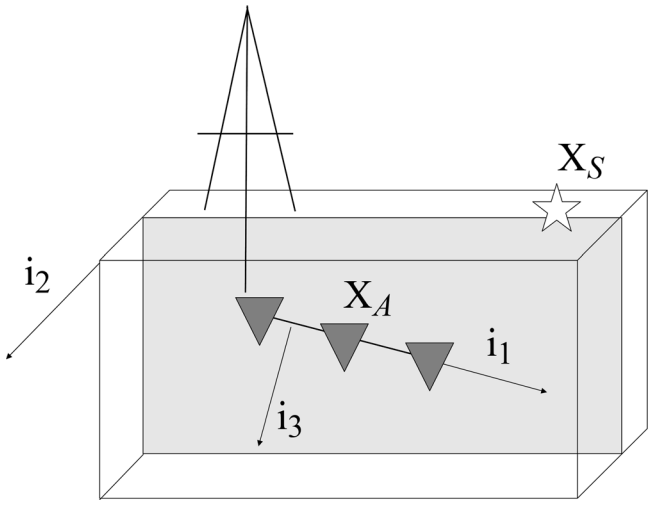

Figure 2. Definition of the Cartesian coordinate frame spanned by normal vectors $\mathbf{i}_1$, $\mathbf{i}_2$, and $\mathbf{i}_3$; $\mathbf{i}_1$ and $\mathbf{i}_3$ define a plane in which the source and receivers are located, where $\mathbf{i}_1$ is parallel to the well.

in equation 2. The overbar indicates that $\bar{\hat{G}}^{-,+}_{m,n}(\mathbf{x}_B,\mathbf{x}_A,\omega)$ is the Green's function of a reference medium where all heterogeneities above the receiver level have been removed. Below the receiver level, the reference medium is identical to the actual medium. No assumptions are imposed on the source component k of the actual sources at $\mathbf{x}_S$. Sources can be force sources or decomposed P- or S-wave sources. Forward problems for MDD can even be derived for simultaneously acting noise sources (Wapenaar and van der Neut, 2010). In equation 4, we have chosen downward-radiating P- and S-wave sources. We solve equation 4 by least-squares inversion. In Appendix C, we show that the implementation of such an inversion is equivalent to solving the following normal equation:

$$\hat{C}^{-,+}_{m,n'}(\mathbf{x}_B,\mathbf{x}'_A,\omega)=\int_{\partial\mathbb{D}_{\mathrm{rec}}}\bar{\hat{G}}^{-,+}_{m,n}(\mathbf{x}_B,\mathbf{x}_A,\omega)\hat{\Gamma}_{n,n'}(\mathbf{x}_A,\mathbf{x}'_A,\omega)d\mathbf{x}_A, \tag{5}$$

where we introduce the correlation function

$$\hat{C}^{-,+}_{m,n'}(\mathbf{x}_B,\mathbf{x}'_A,\omega)=\sum_i\hat{P}^{-,+}_{m,k}(\mathbf{x}_B,\mathbf{x}^{(i)}_S,\omega)\{\hat{P}^{+,+}_{n',k}(\mathbf{x}'_A,\mathbf{x}^{(i)}_S,\omega)\}^* \tag{6}$$

and the interferometric PSF

$$\hat{\Gamma}_{n,n'}(\mathbf{x}_A,\mathbf{x}'_A,\omega)=\sum_i\hat{P}^{+,+}_{n,k}(\mathbf{x}_A,\mathbf{x}^{(i)}_S,\omega)\{\hat{P}^{+,+}_{n',k}(\mathbf{x}'_A,\mathbf{x}^{(i)}_S,\omega)\}^*, \tag{7}$$

with $\mathbf{x}_A$ and $\mathbf{x}'_A$ on $\partial\mathbb{D}_{\mathrm{rec}}$. The correlation function $\hat{C}^{-,+}_{m,n'}(\mathbf{x}_B,\mathbf{x}'_A,\omega)$, defined in equation 6, involves a summation of crosscorrelations of down- and upgoing fields over the sources. It is very similar to a discrete implementation of the right side of equation 2. Therefore, the correlation function itself is close to a representation of the causal Green's function $\hat{G}^{-,+}_{m,n'}(\mathbf{x}_B,\mathbf{x}'_A,\omega)$ minus the acausal Green's function $\{\hat{G}^{+,-}_{n',m}(\mathbf{x}'_A,\mathbf{x}_B,\omega)\}^*$. Alternatively, the correlation function can be interpreted as the desired Green's function $\bar{\hat{G}}^{-,+}_{m,n}(\mathbf{x}_B,\mathbf{x}_A,\omega)$ blurred by the PSF (see equation 5). The PSF can help us diagnose virtual-source defocusing.

Often, a stable multidimensional inverse of the PSF, $\hat{\Gamma}^{\mathrm{inv}}_{n',n''}(\mathbf{x}'_A,\mathbf{x}''_A,\omega)$, can be found, obeying

$$\hat{d}(\mathbf{x}_A-\mathbf{x}''_A)=\int_{\partial\mathbb{D}_{\mathrm{rec}}}\hat{\Gamma}_{n,n'}(\mathbf{x}_A,\mathbf{x}'_A,\omega)\hat{\Gamma}^{\mathrm{inv}}_{n',n''}(\mathbf{x}'_A,\mathbf{x}''_A,\omega)d\mathbf{x}'_A, \tag{8}$$

where $\hat{d}(\mathbf{x}_A-\mathbf{x}''_A)$ is a spatial and temporal band-limited delta function with $\mathbf{x}_A$ and $\mathbf{x}''_A$ on $\partial\mathbb{D}_{\mathrm{rec}}$. Next, we can filter the correlation function with this inverse to remove the PSF imprint from the retrieved data:

$$\begin{aligned}\hat{S}_0(\omega)\bar{\hat{G}}^{-,+}_{m,n''}(\mathbf{x}_B,\mathbf{x}''_A,\omega)&=\hat{S}_0(\omega)\int_{\partial\mathbb{D}_{\mathrm{rec}}}\hat{C}^{-,+}_{m,n'}(\mathbf{x}_B,\mathbf{x}'_A,\omega)\\&\quad\times\hat{\Gamma}^{\mathrm{inv}}_{n',n''}(\mathbf{x}'_A,\mathbf{x}''_A,\omega)d\mathbf{x}'_A,\end{aligned} \tag{9}$$

with $\hat{S}_0(\omega)$ the desired wavelet of the output data. This process, MDD, is implemented to seismic data in the frequency-wavenumber (f-k) domain under an acoustic layered-medium approximation by van der Neut and Bakulin (2009). By obtaining a multidimensional inverse of the PSF, an accurate response can be obtained in general elastic inhomogeneous dissipative media. Recently, MDD has been implemented to virtual crosswell data (Minato et al., 2011), controlled-source electromagnetic (CSEM) exploration (Fan et al., 2009; Hunziker et al., 2009), ground-penetrating radar (GPR) (Slob, 2009), passive seismic interferometry (Wapenaar et al., 2008b), and lithospheric-scale imaging (Ruigrok et al., 2010).

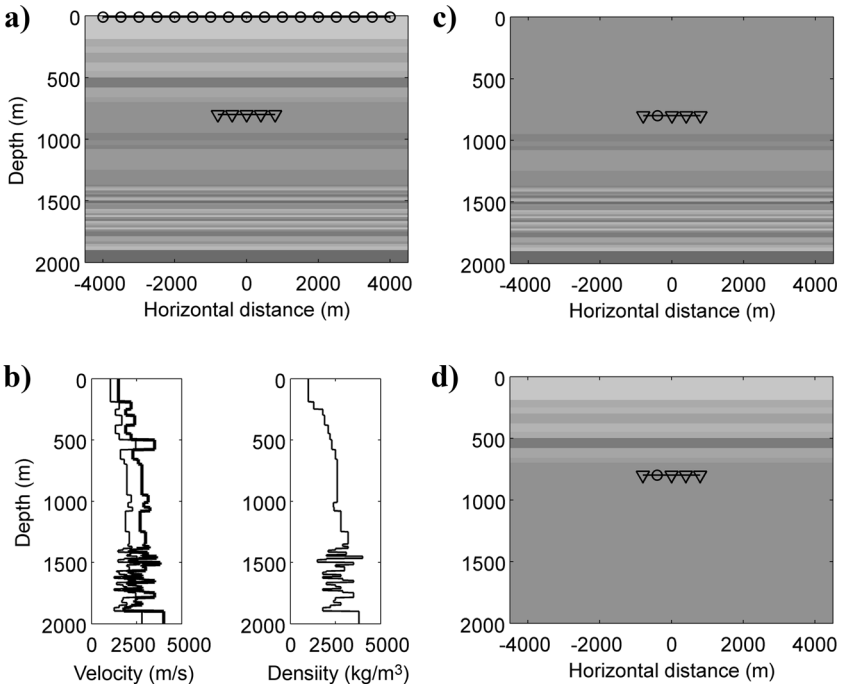

Figure 3. (a) Acquisition: 501 sources (circles) with 16-m spacing are located on the interval [–4000, 4000 m] at 0-m depth, and 101 receivers (triangles) with 16-m spacing are located on the interval [–800, 800 m] at 800-m depth. The P-wave velocities are shown in gray [for exact values, see (b)]. (b) P-wave velocity (solid line), S-wave velocity (dashed line), and density as a function of depth. (c) Acquisition for reference response with medium heterogeneities above the receivers removed; P-wave velocities are shown in gray [for exact values, see (b)]. (d) Acquisition for reference response with medium heterogeneities below the receivers removed; P-wave velocities are shown in gray [for exact values, see (b)].

EXAMPLE 1: LAYERED LOSSLESS MEDIUM

To demonstrate the capabilities of interferometric redatuming by crosscorrelation, we design an idealized elastic 2D example, where all required assumptions (Wapenaar, 2004) are fulfilled. In Figure 3a and 3b, we show the acquisition and elastic medium parameters. At the

earth's surface, 501 two-component (2C) sources (vertical and horizontal force sources) are located with 16-m spacing. In a horizontal well at 800-m depth, 101 four-component (4C) receivers (v_1,v_3,τ_{13}, and τ_{33}) are located with 16-m spacing. We refer to the sources by source numbers 1–501 and the receivers by receiver numbers 1–101, where the central source (251) and the central receiver (51) have zero horizontal offset with respect to each other. No free surface has been incorporated because crosscorrelation-based theory assumes free-surface effects have been removed. A 2D elastic finite-difference code is used (Virieux, 1986), with absorbing boundary conditions applied to the four enclosing boundaries. Below the receiver array, we find a series of layers, providing sufficient backscattering to compensate for the one-sided illumination (Wapenaar, 2006). The medium properties at the receiver level are $\rho(\mathbf{x}_A) = 2600$ kg/m^3, $c_P(\mathbf{x}_A) = 2800$ m/s, and $c_S(\mathbf{x}_A) = 1963$ m/s. The peak frequency is 20 Hz. According to the Nyquist criterion $\Delta x = c_S(\mathbf{x}_A)/2f_C$, spatial aliasing does not occur below $f_C \approx 61$ Hz.

We apply elastic decomposition at the source side to generate downgoing P- and S-wave sources (Wapenaar et al., 1990) and redatum the wavefields from the source level to the receiver level with equation 1. Additional *f-k* filtering is applied to remove artifacts of the decomposition algorithm near and beyond critical angles (horizontal wavenumbers $k_1 \geq \omega/c_P$ are removed during this operation). The band-limited delta function retrieved around $t = 0$ has been muted for visual purposes. We compare the results with a reference response, obtained by placing active force sources at the receiver level and recording the particle velocity responses where the direct field has been muted. The wavelets are aligned with the shaping filter $\hat{F}^k(\mathbf{x}_S, \omega)$, being independent of $\mathbf{x}_S$ in this case. Retrieved virtual-shot gathers and reference responses are shown in Figure 4, where the virtual-source location $\mathbf{x}_A$ has been fixed at receiver 31. The waveforms match in amplitude and phase.

Reflections from above and below the receiver array have been retrieved, which generally is not our desire for further processing. By incorporating elastic decomposition, we can enforce the virtual source to radiate downward or upward only. For this purpose, we decompose the wavefields at the source side and receiver side. To illuminate the medium below the receivers, the downgoing field at $\mathbf{x}_A$ is crosscorrelated with the upgoing field in $\mathbf{x}_B$ (see equation 2). The retrieved response is compared with a reference response obtained by decomposing the full response at the source side and receiver side in a medium without reflectors above the receivers (see Figure 3c). Note that the retrieved Green's function $G^{-,+}_{m,n}(\mathbf{x}_B, \mathbf{x}_A, t)$ can also contain events that have scattered above the receivers. However, such events should have scattered at least three times, making them very weak and insignificant for the present analysis.

In Figure 5, we show virtual shot gathers and reference responses, exposing the reflectors below the receiver array. The waveforms match closely in amplitude and phase, except for the first reflectors at high offsets. Retrieving such events requires high angles of incidence, which are not transmitted from the earth's surface through the heterogeneous overburden. The terminology adopted to describe the wavefields is that the first and second capital symbols denote the wavefields registered at receivers $\mathbf{x}_B$ and emitted at the virtual source $\mathbf{x}_A$, respectively (e.g., PS corresponds to an S-wavefield emitted at $\mathbf{x}_A$ and a P-wavefield registered at $\mathbf{x}_B$).

To image reflectors above the well, we can also generate upward-radiating virtual sources by crosscorrelating the upgoing field at $\mathbf{x}_A$ with the downgoing field at the other receivers (equation 3). A similar processing sequence is implemented, but the reference response is computed in a medium where all reflectors below the receivers have been removed (see Figure 3d). The retrieved responses, $G^{+,-}_{m,n}(\mathbf{x}_B, \mathbf{x}_A, t)$ may still contain interactions with the medium below the receivers, which have scattered at least three times and are neglected in this analysis. In Figure 6, virtual-source gathers and reference responses match almost perfectly , exposing the reflectors above the receiver array. Later in the gather, the retrieved response vanishes because of the limited recording time.

EXAMPLE 2: LAYERED DISSIPATIVE MEDIUM

Earlier, we mentioned several reasons why MDD could be favored over crosscorrelation. One reason is MDD's ability to compensate for intrinsic losses in the medium. To illustrate, we

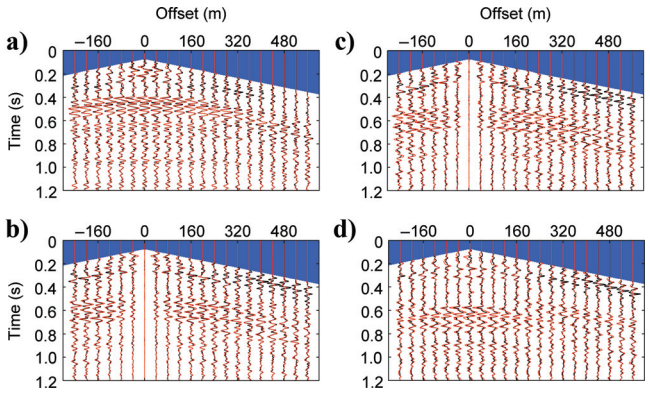

Figure 4. Retrieved virtual-source gathers (red) and reference responses (black) (using equation 1). (a) A virtual vertical-force source at $\mathbf{x}_A$ and vertical particle velocity receivers; (b) a virtual vertical-force source at $\mathbf{x}_A$ and horizontal particle velocity receivers; (c) a virtual horizontal-force source at $\mathbf{x}_A$ and vertical particle velocity receivers; and (d) a virtual horizontal-force source at $\mathbf{x}_A$ and horizontal particle velocity receivers. Every fifth trace is shown. Contributions in the blue area are removed.

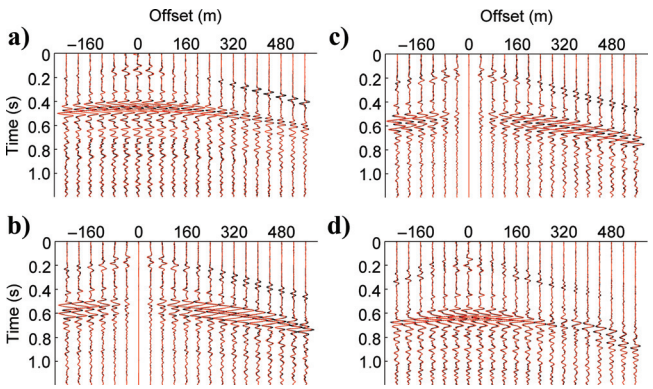

Figure 5. Retrieved virtual-source gathers (red) and reference responses (black) (using equation 2) for a downward-radiating virtual source and receivers for upgoing waves in a lossless medium: (a) PP, (b) SP, (c) PS, (d) SS. Every fifth trace is shown.

generate downgoing virtual sources in the same medium as example 1, with overall quality factors for P-waves $Q_P = 21$ and S-waves $Q_S = 16$ incorporated throughout the medium, using a finite-difference scheme of Robertsson et al. (1994). Because the effects of the losses are visible most severely in the retrieved SS and PS gathers, we concentrate on these.

In Figure 7a and 7b, we show the SS and PS virtual-source gathers (obtained by crosscorrelation, equation 2) and reference responses in the dissipative medium. Misfits of amplitude and phase can be observed. To understand these misfits, we analyze the S-wave PSF in the lossless and dissipative media (see Figure 8a and 8b, respectively). Ideally, these responses would be close to band-limited delta functions, such that the retrieved correlation functions would match the desired reflection responses (equation 5). Note that the PSF in the dissipative medium exposes stronger blurring than the PSF in the lossless medium. This can be observed even better in the *f-k* domain (Figure 9a and 9b). For clarity, late arrivals have been removed in the time-space domain prior to *f-k* transformation. When virtual sources are focused accurately, the *f-k* spectrum of the PSF should be approximately flat within the illuminated cone, corresponding to the desired (band-limited) delta function in the time-space domain (see van der Neut and Bakulin, 2009). In Figure 9a, this is the case in the lossless medium; but in Figure 9b, this is not the case in the dissipative medium.

The defocusing effects caused by intrinsic losses can be removed by implementing MDD (equation 9). In Figure 7c and 7d, we show the virtual-source gathers after MDD and the reference response. The mismatch can no longer be observed. Only reflections at relatively far offsets at early arrival times have not been retrieved because no wavefield passed the overburden with sufficiently high incidence angle. Similar observations are reported by Slob (2009) for redatuming GPR data by MDD.

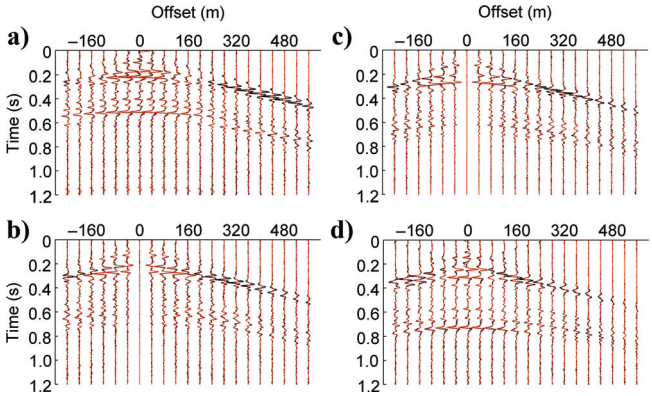

Figure 6. Retrieved virtual-source gathers (red) and reference responses (black) (using equation 3) for an upward-radiating virtual source and receivers for downgoing waves in a lossless medium: (a) PP, (b) SP, (c) PS, (d) SS. Every fifth trace is shown.

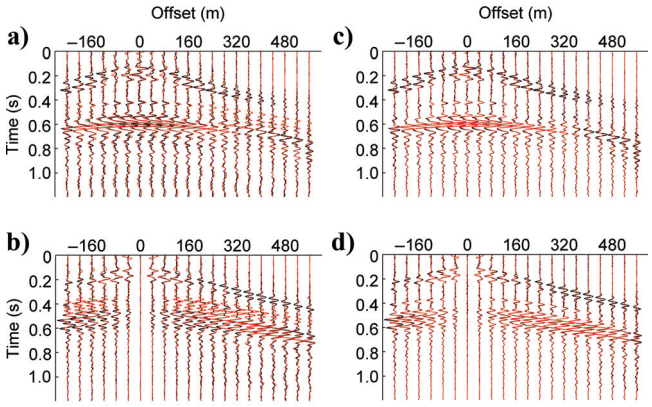

Figure 7. Retrieved virtual-source gathers (red) and reference responses (black) (using equations 2 and 9) for a downward-radiating virtual source and receivers for upgoing waves in a dissipative medium: (a) SS retrieved by crosscorrelation, (b) PS retrieved by crosscorrelation, (c) SS retrieved by MDD, and (d) PS retrieved by MDD. Every fifth trace is shown.

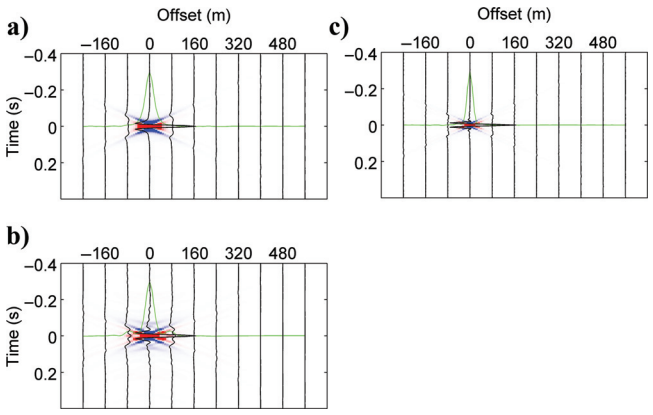

Figure 8. An S-wave PSF in (a) a lossless medium, (b) a dissipative medium before MDD, and (c) a dissipative medium after MDD.

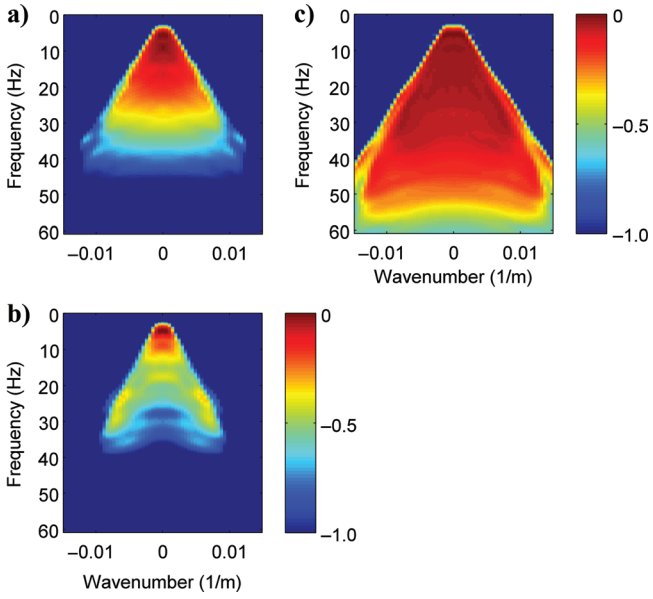

Figure 9. An S-wave PSF in the *f-k* domain in (a) a lossless medium, (b) a dissipative medium before MDD, and (c) a dissipative medium after MDD. All *f-k* spectra are normalized, and the color bar is logarithmic.

Some freedom exists in choosing the stabilization factor of the inversion (see Appendix C). To quantify the effect of MDD on virtual-source focusing, it can be useful to convolve the PSF with its stabilized inverse. We refer to the result of this operation as the PSF after MDD because it provides an indication of improved virtual-source focusing. The S-wave PSF after MDD is shown in Figure 8c; focusing is better than Figure 8b. The *f-k* spectrum of the PSF after MDD is shown in Figure 9c. Note that the spectrum has been flattened considerably compared to Figure 9b. The lower the value of epsilon (equation C-5), the better the focusing at the virtual-source location and the flatter the *f-k* spectrum of the PSF. However, choosing an epsilon too low generally results in inversion artifacts.

EXAMPLE 3: COMPLEX MEDIUM

In the following example, we apply interferometry to redatum multicomponent sources from the earth's surface to multicomponent receiver locations in a deviated well below a complex overburden. The elastic model is a 2D slice taken from a 3D synthetic model inspired by a Shell onshore field in the Middle East (Korneev et al., 2008) (see Figure 10a–10c). Medium properties are not exactly homogeneous at the receiver array (Figure 10d), but average values of $c_P = 1875$ m/s, $c_S = 754$ m/s, and $\rho = 1954$ kg/m^3 are taken for the decomposition algorithm. To allow high-resolution imaging with S-waves, 55 2C force sources are deployed just below (1.5 m) the earth's surface with 60-Hz peak frequency. The source spacing is 12 m, such that a source line of 648 m has been covered. The first five and last five source positions are tapered with a Hanning filter to reduce finite-array artifacts (Mehta et al., 2008). In a deviated well, 128 multicomponent receivers are located, covering an array of approximately 394 m, recording particle velocity and traction. The receiver spacing is chosen relatively small at 3.1 m to avoid spatial aliasing. According to the Nyquist criterion $\Delta x = c_S(\mathbf{x}_A)/2f_C$, aliasing will not occur below $f_C = 120$ Hz, which is about the maximum frequency of the emitted spectrum.

Below the well, we find the finely layered structure that we want to image, having a similar orientation as the well. Because of their relatively short wavelength at 60 Hz, S-waves prove more useful for imaging this target than P-waves. That is why we focus our attention to the retrieved SS reflection response, although we solve the entire elastic system. We create a reference response by placing multicomponent active shots at all receiver locations and applying elastic decomposition at the source side and the receiver side in the *f-k* domain. Because we perform elastic decomposition in the *f-k* domain, whereas the medium properties are not exactly homogeneous at the receiver array (see Figure 10d), neither the redatumed data nor the reference response is exact. Additional *f-k* filtering has been applied because our decomposition algorithm could not handle near-critical angles correctly.

The well and the target reflectors have a dip of about 15° with respect to the earth's surface. The data are rotated to a Cartesian coordinate system with the horizontal and vertical axes parallel and perpendicular to the well, respectively, where the origin coincides with the first receiver location. In Figure 11a, we show the horizontal particle velocity field observed at the receiver array, the result of a horizontal force source (parallel to the earth's surface) in the center of the source array. Gain control has been applied to enhance events at later arrival times. Because of the strong variations in medium properties in the near-subsurface, the recorded wavefields are indeed heavily distorted. We compute the full particle velocity and traction vectors and apply the elastic decomposition scheme discussed in Appendix A. The retrieved upgoing S-wavefield is shown in Figure 11b. Note that part of the downgoing S-wavefield leaked into this gather because the assumption of lateral homogeneity at the receiver level is not exactly fulfilled (Figure 10d).

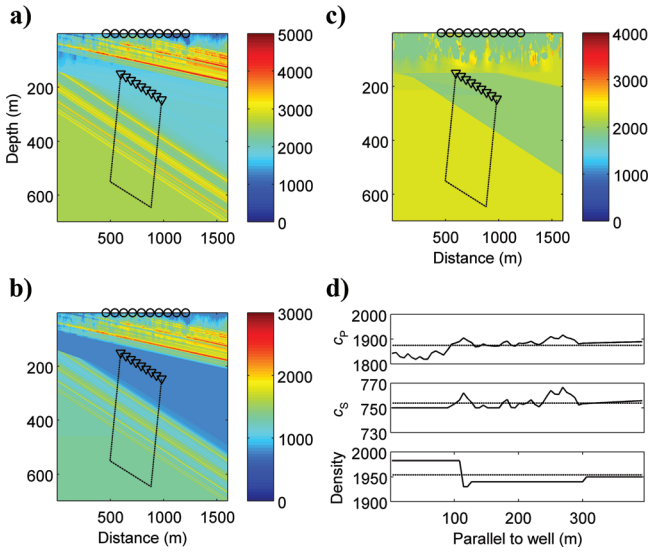

Figure 10. (a) P-wave velocities (in m/s), (b) S-wave velocities (in m/s), and (c) densities (in kg/m^3) of the complex model, with sources (circles) at the earth's surface and receivers (triangles) in a deviated well indicated. The dashed line indicates the target area. (d) P-wave velocity , S-wave velocity c_S, and density at the receiver level (solid lines) and the average values (dashed lines) used in the decomposition scheme.

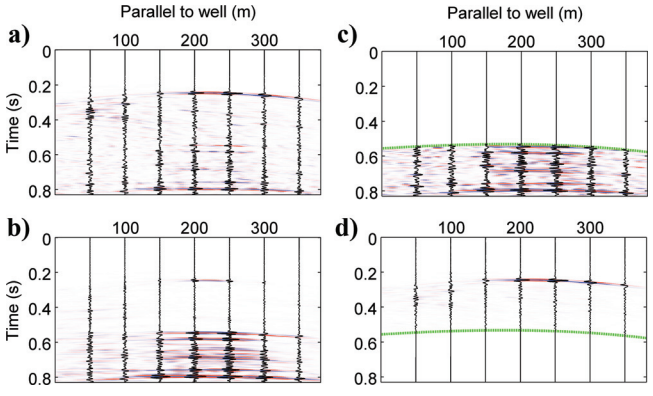

Figure 11. (a) Recorded horizontal particle velocity of a horizontal force source in the center of the source array with gain control applied. (b) Decomposed upgoing S-wavefield obtained with shear traction. (c) Decomposed upgoing S-wavefield obtained without shear traction. (d) Decomposed downgoing S-wavefield obtained without shear traction. In (b-d), no gain control has been applied. Green lines represent time gates. See Appendix D for details.

Next, we implement the alternative elastic decomposition scheme discussed in Appendix D, where we assume the normal traction to be known but the shear traction to be unknown. Figure 11c shows the retrieved upgoing S-wavefield using this scheme. Note that the gather is noisier than in Figure 11b because late downgoing S-waves are handled incorrectly. Early downgoing S-waves, however, are processed well by the scheme, as shown in Figure 11d.

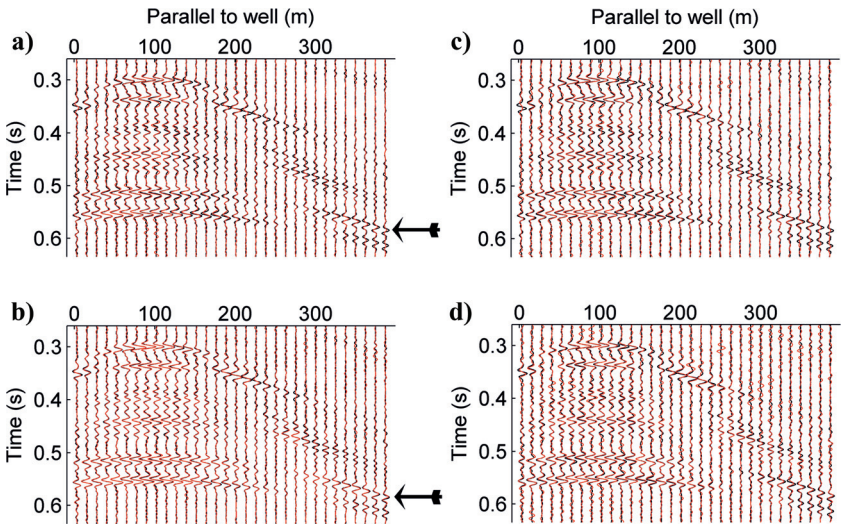

Figure 12. Retrieved virtual source gathers (red) and reference responses (black) (using equations 2 and 9) for a downward-radiating S-wave virtual source and receivers for upgoing S-waves (a) retrieved by crosscorrelation using all components, (b) retrieved by MDD using all components, (c) retrieved by crosscorrelation without shear traction, and (d) retrieved by MDD without shear traction. The arrows indicate the reference reflectors. Every fourth trace is shown.

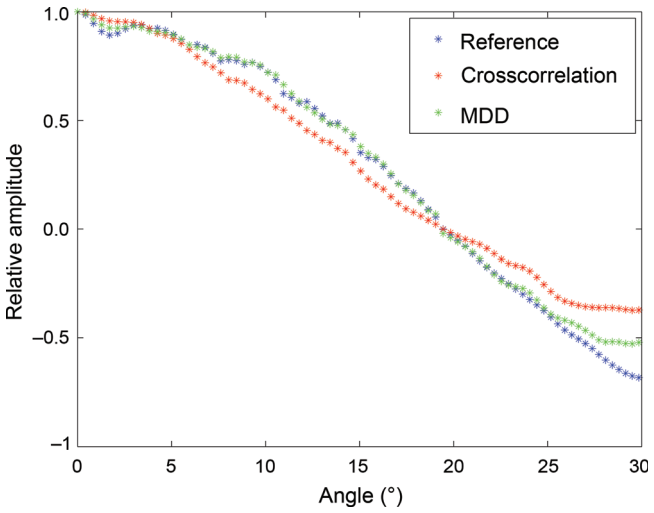

Figure 13. Normalized AVA of a reference reflector (indicated by the arrows in Figure 12) for the reference response (blue), crosscorrelation (red), and MDD (green). Averages have been taken over the receiver array. Small fluctuations are caused mostly by the medium properties along the receiver array, which affect the decomposition of all responses in a similar way. All components have been used in the decomposition algorithm.

We select a reference virtual source location approximately 100 m from the first receiver. In Figure 12a, we show the virtual shot gather at this location retrieved by crosscorrelation and the reference response. The full decomposition scheme (requiring shear traction) has been used. Additional *f-k* filtering is applied to the retrieved response to suppress noise and enforce downward virtual-source radiation. In Figure 12b, we show results from multidimensional deconvolution. The waveform match has improved, and the amplitude spectrum has been reconstructed better.

To demonstrate, we pick the peak amplitudes (normalized by the zero-offset amplitudes) of a reference reflector indicated by the arrows in Figure 12a and 12b. We convert the offsets into angles by ray tracing and correct for geometric spreading by dividing the picked amplitudes with $\sqrt{t_{tw}}$ (t_{tw} being two-way traveltime). Picked values are averaged over the receiver array and normalized as shown in Figure 13 for the reference, crosscorrelation, and MDD responses. Note that MDD is capable of reconstructing the amplitude variation with angle (AVA) behavior very accurately. Only at large angles is the AVA behavior no longer captured.

We repeat the decomposition with the alternative scheme of Appendix D, where the normal traction is assumed to be known but shear traction is unknown. In Figure 12c, we show the response as retrieved by crosscorrelation. Note that the response is slightly noisier than in Figure 12a. Although improvements can be observed after applying MDD, inversion artifacts are also introduced by this strategy (Figure 12d). However, most inversion artifacts appear as uncorrelated noise, which will destructively interfere during migration, as we will see later.

To diagnose virtual-source focusing, we compute the S-wave PSF at the reference virtual-source location (Figure 14a). Indeed, the field is focused at the virtual-source location at $t = 0$. However, some contributions outside of this focus point can be

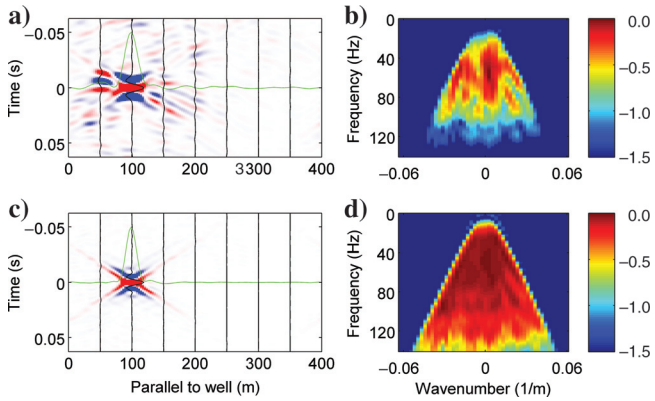

Figure 14. (a) S-wave PSF, (b) *f-k* spectrum of the S-wave PSF, (c) S-wave PSF after MDD, and (d) *f-k* spectrum of the S-wave PSF after MDD. All components have been used in the decomposition algorithm. All *f-k* spectra are normalized. The color bar is logarithmic.

observed. In Figure 14b, we show the PSF in the *f-k* domain. The gather is not entirely flat, as should be the case for perfect focusing. To diagnose the impact of MDD, we show the PSF after this operation (Figure 14c). Note that focusing has improved. A flatter PSF *f-k* spectrum (Figure 14d) also results.

We select a target area in the model, indicated by a dashed black box in Figure 10a–10c. In Figure 15, we show the S-wave reflectivity in the (rotated) target area as computed directly from the S-wave velocity and density model. This reflectivity has been band-pass-filtered to have approximately the same frequency content as the data. One-way wave-equation migration is applied to the retrieved gathers within the target area with a deconvolution-based imaging condition (Thorbecke, 1997). We emphasize that no velocity information outside the target area is required for this operation. In Figure 16a, we show the S-wave image obtained from the responses as retrieved by crosscorrelation. All components have been used in the decomposition scheme. In Figure 16b, we show the image as obtained from MDD data. Note the improved resolution and lateral continuity, especially in the red, yellow, and green boxes indicated in the figures. In Figure 16c, we show the S-wave image that was obtained without shear traction recordings using crosscorrelation. Despite the noisy virtual shot records (Figure 12c), we have still been able to obtain accurate images. The S-wave image obtained from MDD data without shear traction is shown in Figure 16d. Note that improvements over crosscorrelation can still be observed, and much of the noise in the shot records (Figure 12d) has interfered destructively during the migration.

DISCUSSION

All of the examples in this paper are based on 2D elastic wave propagation. Theoretically, to apply MDD in 3D media, one would need a 2D array of receivers in the subsurface. Obviously, this is not feasible in a borehole, where we can sample only in one spatial direction. If medium properties do not vary significantly in the unsampled direction such that P- and SV-waves propagate mainly within a plane spanned by the well and a source line, MDD might still be applied for that single source line. Vasconcelos and Snieder (2008) show that stationary points can be found by trace-to-trace deconvolution and stacking over sources. Similarly, MDD solutions of different source lines might be stacked to find the stationary point in the unsampled direction (perpendicular to the well trajectory). Such a 2.5D approach, which we refer to as line-to-line MDD, is the subject of current research.

In real data applications, acquisition geometries may be less ideal than the ones discussed in this paper. Reducing the number of receivers might result in spatial aliasing problems and, because of limited receiver aperture, the coverage of the integral in equation 4 might be insufficient. Wavefield decomposition can also be problematic because it relies on estimates of the subsurface parameters along the receiver array. In practice, such estimates may be inaccurate, and individual receiver components will need calibration. As for OBC data, an adaptive decomposition scheme might be preferred, in which the medium parameters are estimated during the decomposition process (Schalkwijk et al., 2003). When angles are close to normal incidence, dual-sensor summation may be sufficient (Mehta et al., 2010). In many cases, multicomponent receivers will not be available. If so, approximations to up- and downgoing fields can sometimes be isolated by time gating or (when using vertical boreholes) by *f-k* filtering (Vasconcelos et al., 2008). In such cases, it may be more convenient to speak of

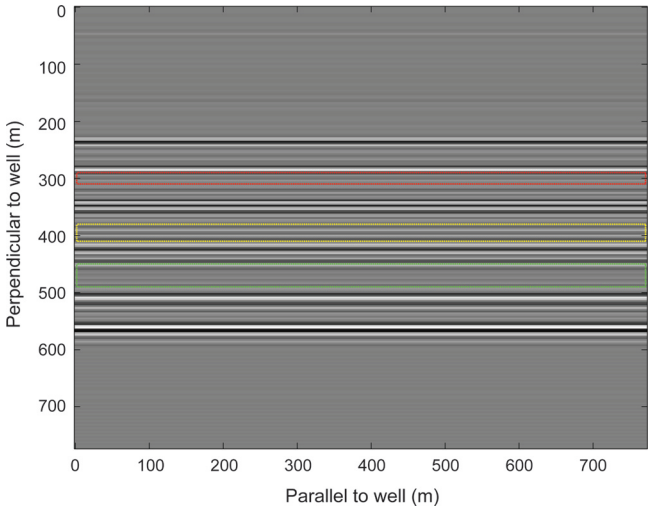

Figure 15. The S-wave reflectivity obtained from S-wave velocity and density models. The red, yellow, and green lines mark parts of the image discussed in the main text.

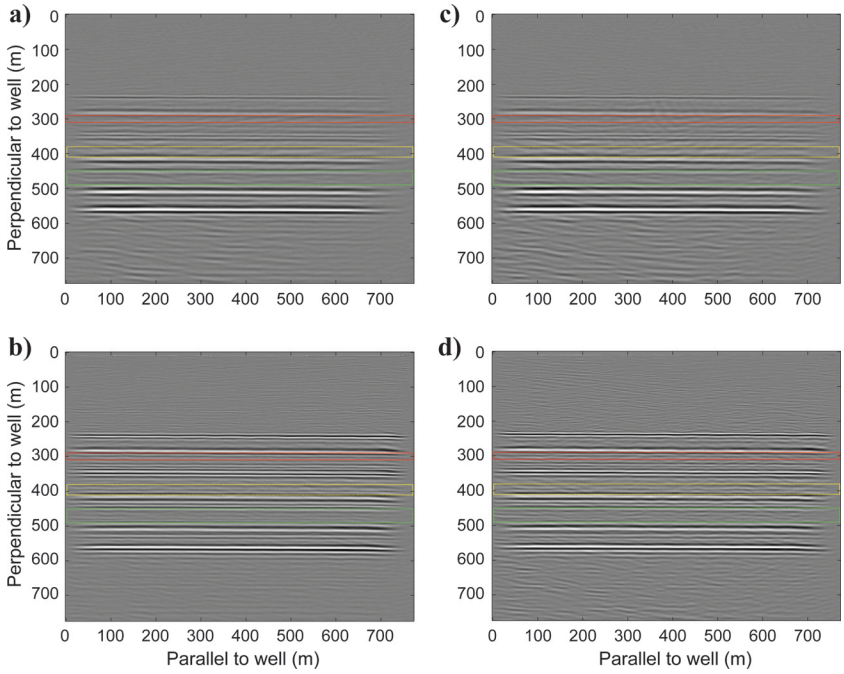

Figure 16. S-wave image obtained from (a) crosscorrelation data using all components, (b) MDD data using all components, (c) crosscorrelation data without shear traction, and (d) MDD data without shear traction. The red, yellow, and green lines mark parts of the image discussed in the main text.

incident (instead of downgoing) and scattered (instead of upgoing) fields and to apply representations for perturbed media (Vasconcelos et al., 2009). Van der Neut (2009) shows that multidimensional deconvolution can also be applied with time-gated fields, leading to a slight change of boundary conditions.

The interferometric PSF has a lot in common with the resolution function or PSF as we find it in seismic migration (Schuster and Hu, 2000; Thorbecke and Wapenaar, 2007; Toxopeus et al., 2008; van Veldhuizen et al., 2008). Interferometry by multidimensional deconvolution as such can be compared with migration deconvolution (Hu et al., 2001; Yu et al., 2006; Zhang and Ulrych, 2010). Such an analogy is also pointed out by Vasconcelos et al. (2010), who present an imaging condition for one-way wavefields that is very similar to equation 4. In migration, the PSF generally has to be obtained from a velocity model, whereas in interferometry it can be computed from actually measured Green's functions, allowing us to focus not only the direct arrival but instead focus the complete wavefield. In this way, spurious events caused by multiple scattering in the overburden can be eliminated efficiently.

CONCLUSION

We have discussed three methods for interferometric redatuming of controlled sources to a downhole receiver array in an elastic medium. Method 1, crosscorrelation of two-way fields, demands little at the receiver side and can be applied even with single-component receivers at single locations. However, this method is demanding at the source side because multicomponent decomposed sources must be evaluated to retrieve exact Green's functions. Moreover, intrinsic losses and free-surface interactions are not accounted for. Similar remarks should be made about method 2, crosscorrelation of one-way fields; it has the additional advantage that virtual sources radiate only downgoing or upgoing P- or S-waves and receivers sense only downgoing or upgoing P- or S-waves. Method 3, MDD, requires sufficient multicomponent receivers to sample a receiver integral. The method is not so demanding at the source side, other than providing sufficient illumination to stabilize the inversion. Free-surface interactions and intrinsic losses are accounted for, and all effects of the overburden, including multiples, are removed. However, the method requires an inversion of the interferometric PSF, which is not always obtained easily in practice. The PSF can also be used to diagnose the quality of data retrieved by crosscorrelation. Convolving the PSF with its stabilized inverse can provide insight in the improved focusing obtained by MDD.

ACKNOWLEDGMENTS

This work is supported by the Dutch Technology Foundation (STW), the Applied Science division of Nederlandse Organisatie voor Wetenschappelljk Onderzoek (NWO), and the Technology Programme of the Ministry of Economic Affairs (grant DCB.7913). We thank Shell E&P for permission to show the elastic model. We also thank Deyan Draganov, Elmer Ruigrok, Juerg Hunziker, Nihed El Allouche (Delft University of Technology), Albena Mateeva (Shell E&P), associate editor Ian Moore (WesternGeco), reviewers Ivan Vasconcelos (Schlumberger) and Andrey Bakulin (Saudi Aramco), and an anonymous reviewer for constructive comments and discussions.

APPENDIX A

ELASTIC DECOMPOSITION IN BOREHOLES

The fundamental quantities to describe elastic wavefields are the particle-velocity vector $\hat{v}_i$ and the stress tensor $\hat{\tau}_{ij}$. In horizontal boreholes, the wavefield is sampled in the $\mathbf{i}_1$-direction only (see Figure 2). For the moment, however, we assume receivers to be present along a plane spanned by $\mathbf{i}_1$ and $\mathbf{i}_2$. We project the stress tensor onto the normal of this plane $\hat{n}_j = \delta_{j3}$ (where δ_{jk} is a Kronecker delta); that is, $\hat{\tau}_{i3} = n_j \hat{\tau}_{ij}$. The quantities $\hat{v}_i$ and $\hat{\tau}_{i3}$ can be combined in the two-way wave vector $\hat{\mathbf{Q}} = (-\hat{\tau}_{13}\ -\hat{\tau}_{23}\ -\hat{\tau}_{33}\ \hat{v}_1\ \hat{v}_2\ \hat{v}_3)^T$, which obeys the two-way wave equation:

$$\partial_3 \hat{\mathbf{Q}} = \hat{\mathbf{A}}\hat{\mathbf{Q}} + \hat{\mathbf{D}}, \tag{A-1}$$

where $\hat{\mathbf{D}}$ is a source vector and where $\hat{\mathbf{A}}$ is a matrix of operators and medium parameters (Frasier, 1970; Ursin, 1983; Wapenaar and Berkhout, 1989). Elastic decomposition can be applied to separate P- and S-wave constituents that are down- and upgoing with respect to the observation plane. This is obtained through eigenvalue decomposition of matrix $\hat{\mathbf{A}} = \hat{\mathbf{L}}\hat{\Lambda}\hat{\mathbf{L}}^{-1}$. The two-way wavefield $\hat{\mathbf{Q}}$ can be decomposed into the one-way wavefield $\hat{\mathbf{P}} = \hat{\mathbf{L}}^{-1}\hat{\mathbf{Q}}$, obeying the one-way wave equation

$$\partial_3 \hat{\mathbf{P}} = \hat{\mathbf{B}}\hat{\mathbf{P}} + \hat{\mathbf{S}}, \tag{A-2}$$

with $\hat{\mathbf{B}} = \hat{\Lambda} - \hat{\mathbf{L}}^{-1}\partial_3\hat{\mathbf{L}}$. Vector $\hat{\mathbf{S}}$ is the decomposed source vector, according to $\hat{\mathbf{S}} = \hat{\mathbf{L}}^{-1}\hat{\mathbf{D}}$. If the medium is laterally homogeneous at the receiver array, decomposition can be obtained in the *f-k* domain (represented by tildes) by inverting $\tilde{\mathbf{L}}\tilde{\mathbf{P}} = \tilde{\mathbf{Q}}$.

Full elastic decomposition would require sampling in two spatial directions of six-component (6C) data. For land data, acquisition is generally performed at the free surface, such that the traction vector vanishes. This allows us to decompose wavefields with 3C geophones only (Dankbaar, 1985; Robertsson and Curtis, 2002). For marine data, if receivers are located at the seafloor, the shear traction components $\tilde{\tau}_{13}$ and $\tilde{\tau}_{23}$ vanish but the normal traction component $\tilde{\tau}_{33}$ does not. By obtaining measurements of the particle velocity vector and the acoustic pressure (which at the seafloor is related to $-\tilde{\tau}_{33}$), elastic decomposition also can be applied in this environment (Amundsen and Reitan, 1995; Schalkwijk et al., 2003; Muijs et al., 2007). For decomposition in boreholes, we are not that fortunate because none of the components of $\tilde{\mathbf{Q}}$ vanishes. This means that, theoretically, 6C data are required along a 2D receiver array.

In practice, we sample the wavefield in the $\mathbf{i}_1$-direction only. Therefore, we apply decomposition in the plane spanned by $\mathbf{i}_1$ and $\mathbf{i}_3$, ignoring out-of-plane reflections. Under this assumption, P- and SV-waves decouple from SH-waves, and 2D elastic decomposition can then be obtained by inverting the following relation:

$$\begin{pmatrix} -\tilde{\tau}_{13} \\ -\tilde{\tau}_{33} \\ \tilde{v}_1 \\ \tilde{v}_3 \end{pmatrix} = \begin{pmatrix} \tilde{L}^+_{1,11} & \tilde{L}^+_{1,12} & \tilde{L}^-_{1,11} & \tilde{L}^-_{1,12} \\ \tilde{L}^+_{1,21} & \tilde{L}^+_{1,22} & \tilde{L}^-_{1,21} & \tilde{L}^-_{1,22} \\ \tilde{L}^+_{2,11} & \tilde{L}^+_{2,12} & \tilde{L}^-_{2,11} & \tilde{L}^-_{2,12} \\ \tilde{L}^+_{2,21} & \tilde{L}^+_{2,22} & \tilde{L}^-_{2,21} & \tilde{L}^-_{2,22} \end{pmatrix} \begin{pmatrix} \tilde{P}^+_{\mathrm{P}} \\ \tilde{P}^+_{\mathrm{S}} \\ \tilde{P}^-_{\mathrm{P}} \\ \tilde{P}^-_{\mathrm{S}} \end{pmatrix}. \tag{A-3}$$

The normal traction can be estimated from downhole pressure measurements, but we do not measure the downhole shear traction.

For this reason, we derived an alternative scheme that does not require the shear traction in Appendix D. For this moment, however, we assume that we record all components, such that equation A-3 can be inverted.

Some freedom exists in scaling the composition matrix $\tilde{\mathbf{L}}$, depending on what we want the decomposed field to represent. Here, we choose to impose flux normalization, meaning that the power flux of the two-way wavefield, $-\tilde{\tau}_{13}^{*}\tilde{v}_1 - \tilde{\tau}_{33}^{*}\tilde{v}_3 - \tilde{v}_1^{*}\tilde{\tau}_{13} - \tilde{v}_3^{*}\tilde{\tau}_{33}$, equals the power flux of the one-way wavefield, $\{\tilde{P}_{\mathrm{P}}^{+}\}^{*}\tilde{P}_{\mathrm{P}}^{+} + \{\tilde{P}_{\mathrm{S}}^{+}\}^{*}\tilde{P}_{\mathrm{S}}^{+} - \{\tilde{P}_{\mathrm{P}}^{-}\}^{*}\tilde{P}_{\mathrm{P}}^{-} - \{\tilde{P}_{\mathrm{S}}^{-}\}^{*}\tilde{P}_{\mathrm{S}}^{-}$ (Frasier, 1970), which allows us to apply one-way reciprocity theorems. An exact representation of $\tilde{\mathbf{L}}$ obeying power-flux normalization is given by Ursin (1983) and Wapenaar et al. (2008a).

In controlled-source interferometry, wave propagation is often close to normal incidence with respect to the well. At normal incidence, it is well known that the decomposition system uncouples because various elements of $\tilde{\mathbf{L}}$ vanish such that equation A-3 can be rewritten as

$$\begin{pmatrix} -\tilde{\tau}_{33} \\ \tilde{v}_3 \end{pmatrix} = \begin{pmatrix} \tilde{L}_{1,21}^{+} & \tilde{L}_{1,21}^{-} \\ \tilde{L}_{2,21}^{+} & \tilde{L}_{2,21}^{-} \end{pmatrix} \begin{pmatrix} \tilde{P}_{\mathrm{P}}^{+} \\ \tilde{P}_{\mathrm{P}}^{-} \end{pmatrix} \tag{A-4}$$

and

$$\begin{pmatrix} -\tilde{\tau}_{13} \\ \tilde{v}_1 \end{pmatrix} = \begin{pmatrix} \tilde{L}_{1,12}^{+} & \tilde{L}_{1,12}^{-} \\ \tilde{L}_{2,12}^{+} & \tilde{L}_{2,12}^{-} \end{pmatrix} \begin{pmatrix} \tilde{P}_{\mathrm{S}}^{+} \\ \tilde{P}_{\mathrm{S}}^{-} \end{pmatrix}. \tag{A-5}$$

In this special case, up- and downgoing P-waves can be described solely by $\tilde{\tau}_{33}$ and $\tilde{v}_3$ (equation A-4), and up- and downgoing S-waves can be described solely by $\tilde{\tau}_{13}$ and $\tilde{v}_1$ (equation A-5). This fact is exploited in the well-known dual-sensor approach, where the P-wave system is decomposed by summing or adding weighted contributions of $\tilde{\tau}_{33}$ and $\tilde{v}_3$, assuming near-normal incidence propagation (Barr, 1997; Mehta et al., 2010). Note that dual-sensor summation can also be applied in the time-space domain, such that an array of sensors is not needed. In the examples in this paper, decomposition is obtained by inverting equation A-3, unless stated differently.

APPENDIX B

GREEN'S FUNCTION REPRESENTATION FOR SEISMIC INTERFEROMETRY BY CROSSCORRELATION OF ONE-WAY WAVEFIELDS

In the following, we decompose Green's functions at the source and receiver sides and cast them in the following matrix:

$$\hat{\mathbf{G}}(\mathbf{x}, \mathbf{x}_S, \omega) = \begin{pmatrix} \hat{G}_{m,k}^{+,+}(\mathbf{x}, \mathbf{x}_S, \omega) & \hat{G}_{m,k}^{+,-}(\mathbf{x}, \mathbf{x}_S, \omega) \\ \hat{G}_{m,k}^{-,+}(\mathbf{x}, \mathbf{x}_S, \omega) & \hat{G}_{m,k}^{-,-}(\mathbf{x}, \mathbf{x}_S, \omega) \end{pmatrix} \tag{B-1}$$

for a source at $\mathbf{x}_S$ and a receiver at $\mathbf{x}$. In $\hat{G}_{m,k}^{\pm,\pm}(\mathbf{x}, \mathbf{x}_S, \omega)$, subscripts m and k refer to different wave modes (P, SV, and SH) at the receiver side (first superscript) and source side (second superscript), respectively. The plus (downgoing) and minus (upgoing) signs denote the propagation direction at the receiver side and source side. All Green's matrices must obey the one-way wave equation A-2, where $\hat{\mathbf{P}}$ is substituted by $\hat{\mathbf{G}}$ and $\hat{\mathbf{S}} = \mathbf{I}\delta(\mathbf{x} - \mathbf{x}_S)$, with $\mathbf{I}$ an identity matrix of the appropriate size and $\delta(\mathbf{x} - \mathbf{x}_S)$ a delta function.

We consider the interaction quantity $\partial_3\{\hat{\mathbf{G}}^{\dagger}(\mathbf{x}, \mathbf{x}_A, \omega)\mathbf{J}\hat{\mathbf{G}}(\mathbf{x}, \mathbf{x}_B, \omega)\}$, where the dagger denotes the complex conjugate transpose, $\mathbf{J} = \begin{pmatrix} \mathbf{I} & \mathbf{0} \\ \mathbf{0} & -\mathbf{I} \end{pmatrix}$, and $\mathbf{0}$ is a matrix of zeros. Next, we apply the product rule for differentiation to the interaction quantity and substitute the one-way wave equation into the result. We integrate over a volume $\mathbb{D}$ enclosed by $\partial\mathbb{D}_{\mathrm{src}}$ and $\partial\mathbb{D}_m$ (Figure 1). Locations $\mathbf{x}_A$ and $\mathbf{x}_B$ are inside the volume of integration. We apply the divergence theorem of Gauss to arrive at

$$\begin{aligned} &\mathbf{J}\hat{\mathbf{G}}(\mathbf{x}_A, \mathbf{x}_B, \omega) + \hat{\mathbf{G}}^{\dagger}(\mathbf{x}_B, \mathbf{x}_A, \omega)\mathbf{J} \\ &\quad = \int_{\partial\mathbb{D}_{\mathrm{src}}+\partial\mathbb{D}_m} \hat{\mathbf{G}}^{\dagger}(\mathbf{x}, \mathbf{x}_A, \omega)\mathbf{J}\hat{\mathbf{G}}(\mathbf{x}, \mathbf{x}_B, \omega) n_3 \, d\mathbf{x} \\ &\quad\quad - \int_{\mathbb{D}} \hat{\mathbf{G}}^{\dagger}(\mathbf{x}, \mathbf{x}_A, \omega)[\hat{\mathbf{B}}^{\dagger}\mathbf{J} + \mathbf{J}\hat{\mathbf{B}}]\hat{\mathbf{G}}(\mathbf{x}, \mathbf{x}_B, \omega) d\mathbf{x}, \end{aligned} \tag{B-2}$$

where n_j is a normal vector perpendicular to the integration boundary, with $n_j = -\delta_{j3}$ at $\partial\mathbb{D}_{\mathrm{src}}$ and $n_j = \delta_{j3}$ at $\partial\mathbb{D}_m$. If sufficient scattering takes place below the receivers, the integration path over $\partial\mathbb{D}_m$ in the first integral can be neglected (Wapenaar, 2006). The volume integral on the right side vanishes if $\hat{\mathbf{B}}^{\dagger}\mathbf{J} = -\mathbf{J}\hat{\mathbf{B}}$, which is the case only if evanescent wavefields are neglected and the medium is free of intrinsic losses.

We transpose equation B-2 and introduce symmetry properties $\mathbf{J}^T = \mathbf{J}^{-1} = \mathbf{J}$, $\hat{\mathbf{G}}^T(\mathbf{x}, \mathbf{x}_A, \omega) = \mathbf{N}\hat{\mathbf{G}}(\mathbf{x}_A, \mathbf{x}, \omega)\mathbf{N}$, where $\mathbf{N} = \begin{pmatrix} \mathbf{0} & \mathbf{I} \\ -\mathbf{I} & \mathbf{0} \end{pmatrix}$, $\mathbf{JN} = -\mathbf{NJ}$, and $\mathbf{N}^{-1} = \mathbf{N}^T = -\mathbf{N}$ to arrive at

$$\begin{aligned} &\hat{\mathbf{G}}(\mathbf{x}_B, \mathbf{x}_A, \omega) + \mathbf{J}\hat{\mathbf{G}}^{\dagger}(\mathbf{x}_A, \mathbf{x}_B, \omega)\mathbf{J} \\ &\quad = \int_{\partial\mathbb{D}_{\mathrm{src}}} \hat{\mathbf{G}}(\mathbf{x}_B, \mathbf{x}_S, \omega)\mathbf{J}\hat{\mathbf{G}}^{\dagger}(\mathbf{x}_A, \mathbf{x}_S, \omega)\,\mathbf{J} d\mathbf{x}_S, \end{aligned} \tag{B-3}$$

where we substituted $\mathbf{x}_S = \mathbf{x}$. Next, we assume that no heterogeneities exist above $\partial\mathbb{D}_{\mathrm{src}}$, such that all relevant wavefields are purely downgoing at the source side. Under this condition, substituting equation B-1 into equation B-3 leads to equations 2 and 3 in the main text. Here, we have assumed that the one-way wavefields can be rewritten as $\hat{P}_{m,k}^{\pm,+}(\mathbf{x}, \mathbf{x}_S, \omega) = \hat{S}^k(\mathbf{x}_S, \omega)\hat{G}_{m,k}^{\pm,+}(\mathbf{x}, \mathbf{x}_S, \omega)$.

Apart from equations 2 and 3, we find two additional equations:

$$\begin{aligned} &\hat{S}_0(\omega)[\hat{G}_{m,n}^{+,+}(\mathbf{x}_B, \mathbf{x}_A, \omega) + \{\hat{G}_{n,m}^{+,+}(\mathbf{x}_A, \mathbf{x}_B, \omega)\}^{*}] \\ &\quad = \int_{\partial\mathbb{D}_{\mathrm{src}}} \hat{F}^k(\mathbf{x}_S, \omega)\hat{P}_{m,k}^{+,+}(\mathbf{x}_B, \mathbf{x}_S, \omega)\{\hat{P}_{n,k}^{+,+}(\mathbf{x}_A, \mathbf{x}_S, \omega)\}^{*} d\mathbf{x}_S \end{aligned} \tag{B-4}$$

and

$$\begin{aligned} &\hat{S}_0(\omega)[\hat{G}_{m,n}^{-,-}(\mathbf{x}_B, \mathbf{x}_A, \omega) + \{\hat{G}_{n,m}^{-,-}(\mathbf{x}_A, \mathbf{x}_B, \omega)\}^{*}] \\ &\quad = -\int_{\partial\mathbb{D}_{\mathrm{src}}} \hat{F}^k(\mathbf{x}_S, \omega)\hat{P}_{m,k}^{-,+}(\mathbf{x}_B, \mathbf{x}_S, \omega)\{\hat{P}_{n,k}^{-,+}(\mathbf{x}_A, \mathbf{x}_S, \omega)\}^{*} d\mathbf{x}_S. \end{aligned} \tag{B-5}$$

Equation B-4 shows that the crosscorrelation of downgoing fields with downgoing fields yields a Green's function as if a downgoing field were emitted at $\mathbf{x}_A$ and a downgoing field were received at $\mathbf{x}_B$. Equation B-5 shows that the crosscorrelation of upgoing fields with upgoing fields yields a Green's function as if an upgoing field were emitted at $\mathbf{x}_A$ and an upgoing field were received at $\mathbf{x}_B$.

APPENDIX C

THE NORMAL EQUATION

We want to invert equation 4 in the main text for $\hat{\tilde{G}}^{-,+}_{m,n}(\mathbf{x}_B,\mathbf{x}_A,\omega)$. For this reason, we define the misfit of this equation as

$$\hat{e}_{m,k}(\mathbf{x}_B,\mathbf{x}_S,\omega)=\hat{P}^{-,+}_{m,k}(\mathbf{x}_B,\mathbf{x}_S,\omega)-\int_{\partial\mathbb{D}_{\text{rec}}}\hat{\tilde{G}}^{-,+}_{m,n}(\mathbf{x}_B,\mathbf{x}_A,\omega)\hat{P}^{+,+}_{n,k}(\mathbf{x}_A,\mathbf{x}_S,\omega)d\mathbf{x}_A. \tag{C-1}$$

In least-squares inversion, we aim to minimize a cost function, defined as (Menke, 1989)

$$\hat{E}_m(\mathbf{x}_B,\omega)=\sum_i\hat{e}_{m,k}(\mathbf{x}_B,\mathbf{x}^{(i)}_S,\omega)\hat{e}^*_{m,k}(\mathbf{x}_B,\mathbf{x}^{(i)}_S,\omega). \tag{C-2}$$

In equation C-2, repeated subscripts m are not implicitly summed over because we aim to invert for each component m separately. Exact minimization of $\hat{E}_m(\mathbf{x}_B,\omega)$ generally results in an unstable solution that is not desired. Numerical instability can be prevented by introducing as an additional constraint the solution length (commonly referred to as regularization):

$$\hat{L}_m(\mathbf{x}_B,\omega)=\int_{\partial\mathbb{D}_{\text{rec}}}\hat{\tilde{G}}^{-,+}_{m,n}(\mathbf{x}_B,\mathbf{x}_A,\omega)\{\hat{\tilde{G}}^{-,+}_{m,n}(\mathbf{x}_B,\mathbf{x}_A,\omega)\}^*d\mathbf{x}_A, \tag{C-3}$$

where subscripts m are once more not implicitly summed over.

Next, for each component m, receiver $\mathbf{x}_B$, and frequency sample ω, we define a separate least-squares minimization problem:

$$\frac{\partial\{\hat{E}_m(\mathbf{x}_B,\omega)+\varepsilon^2\hat{L}_m(\mathbf{x}_B,\omega)\}}{\partial\hat{\tilde{G}}^{-,+}_{m,n}(\mathbf{x}_B,\mathbf{x}_A,\omega)}=0, \tag{C-4}$$

where ε is introduced to control the balance between minimizing $\hat{E}_m(\mathbf{x}_B,\omega)$ (low ε) and $\hat{L}_m(\mathbf{x}_B,\omega)$ (high ε). Via some algebra (Menke, 1989), equation C-4 can be rewritten as the following normal equation:

$$\hat{C}^{-,+}_{m,n'}(\mathbf{x}_B,\mathbf{x}'_A,\omega)=\int_{\partial\mathbb{D}_{\text{rec}}}\hat{\tilde{G}}^{-,+}_{m,n}(\mathbf{x}_B,\mathbf{x}_A,\omega)[\hat{\Gamma}_{n,n'}(\mathbf{x}_A,\mathbf{x}'_A,\omega)+\varepsilon^2\delta(\mathbf{x}_A-\mathbf{x}'_A)\delta_{nn'}]d\mathbf{x}_A, \tag{C-5}$$

where $\delta_{nn'}$ is a Kronecker delta function and where $\hat{C}^{-,+}_{m,n'}(\mathbf{x}_B,\mathbf{x}'_A,\omega)$ and $\hat{\Gamma}_{n,n'}(\mathbf{x}_A,\mathbf{x}'_A,\omega)$ are defined in equations 6 and 7. Setting $\varepsilon=0$, equation C-5 turns into equation 4. However, to obtain a stable solution, we generally must include $\varepsilon>0$ in the inversion of equation C-5.

APPENDIX D

ELASTIC DECOMPOSITION IN BOREHOLES WITHOUT SHEAR TRACTION

Recall from equation A-3 that four receiver components are required to implement 2D elastic decomposition in boreholes. In multicomponent surveys, particle velocities $\tilde{v}_1$ and $\tilde{v}_3$ are recorded. In modern surveys, downhole hydrophones also tend to be deployed, from which an approximation of the normal traction $\tilde{\tau}_{33}$ can be estimated (Mehta et al., 2010). However, the shear traction $\tilde{\tau}_{13}$ is generally unknown; therefore, the elastic decomposition problem is underdetermined with three equations and four unknowns.

To overcome this problem, we introduce an additional constraint by replacing $\tilde{\tau}_{13}$ and the first row in matrix $\tilde{\mathbf{L}}$ with coefficients $\tilde{A}$, $\tilde{C}^{\pm}_{\text{P}}$, and $\tilde{C}^{\pm}_{\text{S}}$:

$$\begin{pmatrix}\tilde{A}\\-\tilde{\tau}_{33}\\\tilde{v}_1\\\tilde{v}_3\end{pmatrix}=\begin{pmatrix}\tilde{C}^+_{\text{P}}&\tilde{C}^+_{\text{S}}&\tilde{C}^-_{\text{P}}&\tilde{C}^-_{\text{S}}\\\tilde{L}^+_{1,21}&\tilde{L}^+_{1,22}&\tilde{L}^-_{1,21}&\tilde{L}^-_{1,22}\\\tilde{L}^+_{2,11}&\tilde{L}^+_{2,12}&\tilde{L}^-_{2,11}&\tilde{L}^-_{2,12}\\\tilde{L}^+_{2,21}&\tilde{L}^+_{2,22}&\tilde{L}^-_{2,21}&\tilde{L}^-_{2,22}\end{pmatrix}\begin{pmatrix}\tilde{P}^+_{\text{P}}\\\tilde{P}^+_{\text{S}}\\\tilde{P}^-_{\text{P}}\\\tilde{P}^-_{\text{S}}\end{pmatrix}. \tag{D-1}$$

Because $\tilde{\tau}_{13}$ is not recorded, separation of up- and downgoing S-waves is impossible at normal incidence (see equation A-5). Interferometric redatuming requires good separation near or close to normal incidence, so the imposed constraint should in some way introduce the separation of up- and downgoing S-waves to the decomposition system. We notice that upgoing S-waves generally arrive relatively late with respect to the other components. For early arrival times, a reasonable assumption seems that no upgoing S-waves exist; in other words, $\tilde{P}^-_{\text{S}}=0$. This assumption can be introduced in equation D-1 by the coefficients defined in Table D-1, yielding a system of four equations and four unknowns that can be inverted. In our experience, the assumption $\tilde{P}^-_{\text{S}}=0$ allows us to discriminate well between up- and downgoing P-waves throughout the gathers. For S-waves, we must adopt a different strategy.

Table D-1. Coefficients for different assumptions.

Assumption	$\tilde{A}$	$\tilde{C}^+_{\text{P}}$	$\tilde{C}^+_{\text{S}}$	$\tilde{C}^-_{\text{P}}$	$\tilde{C}^-_{\text{S}}$
$\tilde{P}^-_S=0$	0	0	0	0	1
$\tilde{P}^+_S=0$	0	0	1	0	0

The first significant upgoing S-wavefield can often be distinguished by visual inspection. We place a time gate right above this event. For the upper part (early arrival times) of the data, we adapt the $\tilde{P}^-_{\text{S}}=0$ assumption to retrieve the downgoing S-wavefield. For the lower part (late arrival times) of the data, we assume that no downgoing S-wave is present, which is imposed by a $\tilde{P}^+_{\text{S}}=0$ assumption, introduced by the coefficients as given in Table D-1. Downgoing S-waves often exist in the lower part, especially stemming from interactions with the free surface (multiples). For the complex model we consider in example 3, the $\tilde{P}^+_{\text{S}}=0$ assumption appears relatively successful in extracting the dominant upgoing S-wave. For different data sets, alternative constraints may be preferred.

REFERENCES

Amundsen, L., L. T. Ikelle, and L. E. Berg, 2001, Multidimensional signature deconvolution and free-surface multiple elimination of marine multicomponent ocean-bottom seismic data: Geophysics, **66**, 1594–1604, doi:10.1190/1.1486770.

Amundsen, L., and A. Reitain, 1995, Decomposition of multicomponent sea-floor data into upgoing and downgoing P- and S-waves: Geophysics, **60**, 563–572, doi:10.1190/1.1443794.
Bakulin, A., and R. Calvert, 2006, The virtual source method: Theory and case study: Geophysics, **71**, no. 4, SI139–SI150, doi:10.1190/1.2216190.
Bakulin, A., A. Mateeva, R. Calvert, P. Jorgensen, and J. Lopez, 2007a, Virtual shear source makes shear waves with air guns: Geophysics, **72**, no. 2, A7–A11, doi:10.1190/1.2430563.
Bakulin, A., A. Mateeva, K. Mehta, P. Jorgensen, J. Ferrandis, I. S. Herhold, and J. Lopez, 2007b, Virtual source applications to imaging and reservoir monitoring: The Leading Edge, **26**, 732–740, doi:10.1190/1.2748490.
Barr, F. J., 1997, Dual-sensor OBC technology: The Leading Edge, **16**, 45–51, doi:10.1190/1.1437427.
Berkhout, A. J., 1997, Pushing the limits of seismic imaging, Part I: Prestack migration in terms of double dynamic focusing: Geophysics, **62**, 937–954.
Berryhill, J. R., 1979, Wave-equation datuming: Geophysics, **44**, 1329–1344, doi:10.1190/1.1441010.
Dankbaar, J. W. M., 1985, Separation of P- and S-waves: Geophysical Prospecting, **33**, 970–986, doi:10.1111/j.1365-2478.1985.tb00792.x.
Fan, Y., R. Snieder, J., and Singer, 2009, 3D controlled source electromagnetic (CSEM) interferometry by multidimensional deconvolution: 79th Annual International Meeting, SEG, Expanded Abstracts, 779–783.
Frasier, C. W., 1970, Discrete time solution of plane P-SV waves in a plane layered medium: Geophysics, **35**, 197–219, doi:10.1190/1.1440085.
Frijlink, M., and K. Wapenaar, 2010, Reciprocity theorems for one-way wave fields in curvilinear coordinate systems: SIAM Journal on Imaging Sciences, **3**, 390–415, doi:10.1137/080739185.
Gaiser, J. E., and I. Vasconcelos, 2010, Elastic interferometry for ocean bottom cable data: Theory and examples: Geophysical Prospecting, **58**, 347–360, doi:10.1111/j.1365-2478.2009.00825.x.
Gaiser, J. E., I. Vasconcelos, and R. Ramkhelawan, 2009, Elastic-wavefield interferometry — Pseudo-source VSPs from 3D P-wave vibrator data, Wamsutter field, WY, USA: 71st Annual Conference & Technical Exhibition, EAGE, Extended Abstracts, T037.
Holvik, E., and L. Amundsen, 2005, Elimination of the overburden response from multicomponent source and receiver seismic data, with source designature and decomposition into PP-, PS-, SP-, and SS-wave responses: Geophysics, **70**, no. 2, S43–S59, doi:10.1190/1.1897037.
Hu, J., G. T. Schuster, and P. Valasek, 2001, Poststack migration deconvolution: Geophysics, **66**, 939–952, doi:10.1190/1.1444984.
Hunziker, J., E. C. Slob, and K. Wapenaar, 2009, Controlled source electromagnetic interferometry by multidimensional deconvolution — Spatial sampling aspects: 71st Annual Conference & Technical Exhibition, EAGE, Extended Abstracts, P074.
Kelamis, P. G., K. E. Erickson, D. J. Verschuur, and A. J. Berkhout, 2002, Velocity-independent redatuming: A new approach to the near-surface problem in land seismic data processing: The Leading Edge, **21**, 730–735, doi:10.1190/1.1503185.
Korneev, V., and A. Bakulin, 2006, On the fundamentals of the virtual source method: Geophysics, **71**, no. 3, A13–A17, doi:10.1190/1.2196868.
Korneev, V., A. Bakulin, and J. Lopez, 2008, Imaging and monitoring with virtual sources on a synthetic 3D data set from the Middle East: 78th Annual International Meeting, SEG, Expanded Abstracts, 3204–3208.
Leaney, W. S., 1990, Parametric wavefield decomposition and applications: 60th Annual International Meeting, SEG, Expanded Abstracts, 1097–1101.
Mehta, K., A. Bakulin, J. Sheiman, R. Calvert, and R. Snieder, 2007, Improving the virtual source method by wavefield separation: Geophysics, **72**, no. 4, V79–V86, doi:10.1190/1.2733020.
Mehta, K., D. Kiyashchenko, P. Jorgensen, J. Lopez, J. Ferrandis, and M. Costello, 2010, Virtual source method applied to crosswell and horizontal well geometries: The Leading Edge, **29**, 712–723, doi:10.1190/1.3447785.
Mehta, K., R. Snieder, R. Calvert, and J. Sheiman, 2008, Acquisition geometry requirements for generating virtual-source data: The Leading Edge, **27**, 620–629, doi:10.1190/1.2919580.
Menke, W., 1989, Geophysical data analysis: Academic Press.
Minato, S., T. Matsuoka, T. Tsuji, D. Draganov, J. Hunziker, and K. Wapenaar, 2011, Seismic interferometry using multidimensional deconvolution and crosscorrelation for crosswell seismic reflection data without borehole sources: Geophysics, **76**, no. 1, SA19–SA34, doi:10.1190/1.3511357.
Muijs, R., J. O. A. Robertsson, and K. Holliger, 2007, Data-driven adaptive decomposition of multicomponent seabed seismic recordings: Application to shallow-water data from the North Sea: Geophysics, **72**, no. 6, V133–V142, doi:10.1190/1.2778766.
Mulder, W. A., 2005, Rigorous redatuming: Geophysical Journal International, **161**, 401–415, doi:10.1111/j.1365-246X.2005.02615.x.
Poletto, F., P. Corubolo, and P. Comelli, 2010, Drill-bit seismic interferometry with and without pilot signals: Geophysical Prospecting, **58**, no. 2, 257–265, doi:10.1111/j.1365-2478.2009.00832.x.
Poletto, F., L. Petronio, B. Farina, and A. Schleifer, 2008, Single well imaging in cased borehole by interferometry: 70th Annual Conference & Technical Exhibition, EAGE, Extended Abstracts, P278.
Robertsson, J. O. A., J. O. Blanch, and W. W. Symes, 1994, Viscoelastic finite-difference modeling: Geophysics, **59**, 1444–1456, doi:10.1190/1.1443701.
Robertsson, J. O. A., and A. Curtis, 2002, Wavefield separation using densely deployed, three component, single sensor groups in land surface seismic recordings: Geophysics, **67**, 1624–1633, doi:10.1190/1.1512809.
Ruigrok, E., J. van der Neut, H. Djikpesse, C. Chen, and K. Wapenaar, 2010, A feasibility study for the application of seismic interferometry of multidimensional deconvolution for lithospheric-scale imaging: European Geophysical Union General Assembly Geophysical Research Abstracts, EGU9370.
Schalkwijk, K. M., C. P. A. Wapenaar, and D. J. Verschuur, 2003, Adaptive decomposition of multicomponent ocean-bottom seismic data into downgoing and upgoing P- and S-waves: Geophysics, **68**, 1091–1102, doi:10.1190/1.1581081.
Schuster, G. T., 2009, Seismic interferometry: Cambridge University Press.
Schuster, G. T., and J. Hu, 2000, Green's function for migration: Continuous recording geometry: Geophysics, **65**, 167–175, doi:10.1190/1.1444707.
Schuster, G. T., and M. Zhou, 2006, A theoretical overview of model-based and correlation-based redatuming methods: Geophysics, **71**, no. 4, SI103–SI110, doi:10.1190/1.2208967.
Slob, E., 2009, Interferometry by deconvolution of multi-component multi-offset GPR data: IEEE Transactions on Geoscience and Remote Sensing, **47**, no. 3, 828–838, doi:10.1109/TGRS.2008.2005250.
Snieder, R., 2007, Extracting the Green's function of attenuating heterogeneous acoustic media from uncorrelated waves: Journal of the Acoustical Society of America, **121**, 2637–2643, doi:10.1121/1.2713673.
Snieder, R., J. Sheiman, and R. Calvert, 2006, Equivalence of the virtual source method and wavefield deconvolution in seismic interferometry: Physical Review E, **73**, 066620, doi:10.1103/PhysRevE.73.066620.
Sun, W., S. Z. Sun, and H. Bai, 2009, 3C-3D VSP vector wavefield separation with constrained inversion: 79th Annual International Meeting, SEG, Expanded Abstracts, 4080–4084.
Tegtmeier, S., A. Gisolf, and D. J. Verschuur, 2004, 3D sparse-data Kirchhoff redatuming: Geophysical Prospecting, **52**, 509–521, doi:10.1111/j.1365-2478.2004.00443.x.
Thorbecke, J., 1997, Common focus point technology: Ph.D. dissertation, Delft University of Technology.
Thorbecke, J., and K. Wapenaar, 2007, On the relation between seismic interferometry and migration resolution function: Geophysics, **72**, no. 6, T61–T66, doi:10.1190/1.2785850.
Toxopeus, G., J. Thorbecke, K. Wapenaar, S. Petersen, E. Slob, and J. Fokkema, 2008, Simulating migrated and inverted seismic data by filtering a geologic model: Geophysics, **73**, no. 2, T1–T10, doi:10.1190/1.2827875.
Ursin, B., 1983, Review of elastic and electromagnetic wave propagation in horizontally layered media: Geophysics, **48**, 1063–1081, doi:10.1190/1.1441529.
van der Neut, J., 2009, Seismic interferometry by multidimensional deconvolution with time-gated fields: 71st Annual Conference & Technical Exhibition, EAGE, Extended Abstracts, X041.
van der Neut, J., and A. Bakulin, 2009, Estimating and correcting the amplitude radiation pattern of a virtual source: Geophysics, **74**, no. 2, SI27–SI36, doi:10.1190/1.3073003.
van Manen, D. J., A. Curtis, and J. O. A. Robertsson, 2006, Interferometric modeling of wave propagation in inhomogeneous elastic media using time reversal and reciprocity: Geophysics, **71**, no. 4, SI47–SI60, doi:10.1190/1.2213218.
van Veldhuizen, E. J., G. Blacquière, and A. J. Berkhout, 2008, Acquisition geometry analysis in complex 3D media: Geophysics, **73**, no. 5, Q43–Q58, doi:10.1190/1.2972029.
Vasconcelos, I., P. Sava, and H. Douma, 2010, Nonlinear extended images via image-domain interferometry: Geophysics, **75**, no. 6, SA105–SA115, doi:10.1190/1.3494083.
Vasconcelos, I., and R. Snieder, 2008, Interferometry by deconvolution, Part 2: Theory for elastic waves and application to drill-bit seismic imaging: Geophysics, **73**, no. 3, S129–S141, doi:10.1190/1.2904985.
Vasconcelos, I., R. Snieder, and H. Douma, 2009, Representation theorems and Green's function retrieval for scattering in acoustic media: Physical Review E, **80**, no. 3, 036605, doi:10.1103/PhysRevE.80.036605.

Vasconcelos, I., R. Snieder, and B. Hornby, 2008, Imaging internal multiples from subsalt VSP data — Examples of target-oriented interferometry: Geophysics, **73**, no. 4, S157–S168, doi:10.1190/1.2944168.

Virieux, J., 1986, P-SV wave propagation in heterogeneous media: Velocity-stress finite-difference method: Geophysics, **51**, 889–901, doi:10.1190/1.1442147.

Wapenaar, K., 2004, Retrieving the elastodynamic Green's function of an arbitrary inhomogeneous medium by cross correlation: Physical Review Letters, **93**, no. 25, 254301, doi:10.1103/PhysRevLett.93.254301.

———, 2006, Green's function retrieval by cross-correlation in case of one-sided illumination: Geophysical Research Letters, **33**, no. 19, L19304, doi:10.1029/2006GL027747.

Wapenaar, C. P. A., and A. J. Berkhout, 1989, Elastic wave field extrapolation: Redatuming of single- and multi-component seismic data: Elsevier Science Publ. Co., Inc.

Wapenaar, C. P. A., P. Herrmann, D. J. Verschuur, and A. J. Berkhout, 1990, Decomposition of multi-component seismic data into primary P- and S-wave responses: Geophysical Prospecting, **38**, 633–661, doi:10.1111/j.1365-2478.1990.tb01867.x.

Wapenaar, K., E. Slob, and R. Snieder, 2008a, Seismic and electromagnetic controlled-source interferometry in dissipative media: Geophysical Prospecting, **56**, 419–434, doi:10.1111/j.1365-2478.2007.00686.x.

Wapenaar, K., and J. van der Neut, 2010, A representation for Green's function retrieval by multidimensional deconvolution: Journal of the Acoustical Society of America, **128**, no. 6, EL366–EL371, doi:10.1121/1.3509797.

Wapenaar, K., J. van der Neut, and E. Ruigrok, 2008b, Passive seismic interferometry by multidimensional deconvolution: Geophysics, **73**, no. 6, A51–A56, doi:10.1190/1.2976118.

Xiao, X., M. Zhou, and G. T. Schuster, 2006, Salt-flank delineation by interferometric imaging of transmitted P- to S-waves: Geophysics, **71**, no. 4, SI197–SI207, doi:10.1190/1.2209550.

Yu, J., J. Hu, G. T. Schuster, and R. Estill, 2006, Prestack migration deconvolution: Geophysics, **71**, no. 2, S53–S62, doi:10.1190/1.2187783.

Zhang, C., and T. J. Ulrych, 2010, Refocusing migrated seismic images in absorptive media: Geophysics, **75**, no. 3, S103–S110, doi:10.1190/1.3374434.